Inorganic Chemistry
Cite This: Inorg. Chem. XXXX, XXX, XXX−XXX
Article
pubs.acs.org/IC

Quasi-2D Heisenberg Antiferromagnets $[CuX(pyz)_2](BF_4)$ with X = Cl and Br

Mariusz Kubus,[†,‡] Arianna Lanza,[†,§] Rebecca Scatena,[†] Leonardo H. R. Dos Santos,[†] Björn Wehinger,[‡,#] Nicola Casati,[§] Christoph Fiolka,[†] Lukas Keller,[‡] Piero Macchi,[*,†] Christian Rüegg,[*,‡,#] and Karl W. Krämer[*,†]

[†]Department of Chemistry and Biochemistry, University of Bern, Freiestrasse 3, CH-3012 Bern, Switzerland
[‡]Laboratory for Neutron Scattering and Imaging and [§]Laboratory for Synchrotron Radiation−Condensed Matter, Paul Scherrer Institute, CH-5232 Villigen PSI, Switzerland
[#]Department of Quantum Matter Physics, University of Geneva, Quai Ernest Ansermet 24, CH-1211 Genève 4, Switzerland

Supporting Information

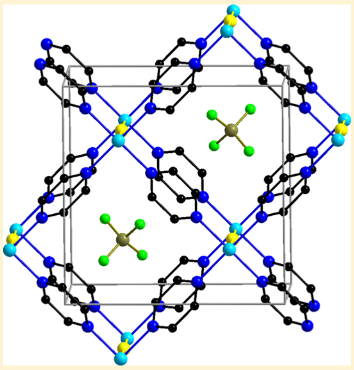

ABSTRACT: Two Cu^{2+} coordination polymers $[CuCl(pyz)_2](BF_4)$ **1** and $[CuBr(pyz)_2](BF_4)$ **2** (pyz = pyrazine) were synthesized in the family of quasi two-dimensional (2D) $[Cu(pyz)_2]^{2+}$ magnetic networks. The layer connectivity by monatomic halide ligands results in significantly shorter interlayer distances. Structures were determined by single-crystal X-ray diffraction. Temperature-dependent X-ray diffraction of **1** revealed rigid $[Cu(pyz)_2]^{2+}$ layers that do not expand between 5 K and room temperature, whereas the expansion along the *c*-axis amounts to 2%. The magnetic susceptibility of **1** and **2** shows a broad maximum at ~8 K, indicating antiferromagnetic interactions within the $[Cu(pyz)_2]^{2+}$ layers. 2D Heisenberg model fits result in $J_{\parallel} = 9.4(1)$ K for **1** and 8.9(1) K for **2**. The interlayer coupling is much weaker with $|J_{\perp}| = 0.31(6)$ K for **1** and 0.52(9) K for **2**. The electron density, experimentally determined and calculated by density functional theory, confirms the location of the singly occupied orbital (the magnetic orbital) in the tetragonal plane. The analysis of the spin density reveals a mainly σ-type exchange through pyrazine. Kinks in the magnetic susceptibility indicate the onset of long-range three-dimensional magnetic order below 4 K. The magnetic structures were determined by neutron diffraction. Magnetic Bragg peaks occur below $T_N = 3.9(1)$ K for **1** and 3.8(1) K for **2**. The magnetic unit cell is doubled along the *c*-axis ($\mathbf{k} = 0, 0, 0.5$). The ordered magnetic moments are located in the tetragonal plane and amount to $0.76(8)\ \mu_B/Cu^{2+}$ for **1** and $0.6(1)\ \mu_B/Cu^{2+}$ for **2** at 1.5 K. The moments are coupled antiferromagnetically both in the *ab* plane and along the *c*-axis. The Cu^{2+} *g*-tensor was determined from electron spin resonance spectra as $g_x = 2.060(1)$, $g_z = 2.275(1)$ for **1** and $g_x = 2.057(1)$, $g_z = 2.272(1)$ for **2** at room temperature.

INTRODUCTION

Quasi two-dimensional (2D) $S = 1/2$ square-lattice Heisenberg antiferromagnets (AFM) have attracted much attention in recent years as magnetic model systems due to their relation to high-temperature cuprate superconductors,[1−3] their quantum fluctuations below Néel temperature (T_N), and a possible application in quantum computing.[4−6] Molecular magnets play a major role in this field.[7−9] Their versatile composition from metal ions as spin carriers and ligands as linkers allows the design of tailored lattices for magnetic model systems.[10,11] Composition, configuration geometry, and conjugation of the linkers influence the exchange between magnetic centers. Often studied are systems with short linkers, for example, O^{2-}, OH^-, N^{3-}, or conjugated groups, such as oxalate or pyrazine (pyz).[10,12] The search for new magnetic materials for experimental and theoretical investigations can be based on modifications of known compounds, for example, the single and double layer models $[CuF_2(H_2O)_2(pyz)]$[13] and $[(CuF_2(H_2O)_2)_2(pyz)]$,[14] respectively, or the exploration of new systems. Cu^{2+} ions with their small $S = 1/2$ spin are of particular interest in quantum magnetism. Coordination compounds are rather soft and susceptible to the application of external pressure, which may induce structural or magnetic phase transitions.[15] The relatively weak magnetic interactions in these 2D Cu^{2+} materials result in moderate saturation fields at low temperature,[16] which are experimentally accessible and allow a direct determination of the coupling parameters by inelastic neutron scattering.

The family of $[CuX(pyz)_2]Y$ compounds has attracted major attention in this field. These compounds are based on $[Cu(pyz)_2]^{2+}$ layers that are bridged in the third dimension by X ligands, and charge is compensated by Y anions. Their three-dimensional (3D) coordination network hosts quasi 2D magnetic interactions. As examples, X can be NO_3^- and Y = PF_6^-,[16] or X = HF_2^- and Y = ClO_4^-,[4] BF_4^-,[17] PF_6^-,[4] SbF_6^-,[18] AsF_6^-,[4] or TaF_6^-.[19]

Received: December 19, 2017

DOI: 10.1021/acs.inorgchem.7b03150
Inorg. Chem. XXXX, XXX, XXX−XXX

Data available in literature do not allow an easy rationalization of the magnetic exchange in this family of compounds. In particular, the role of interlayer interactions through X anions or the role of the counterion Y remain unclear. For this reason, we synthesized further compounds and characterized their structure/property relationships. Here, we present two members of the $[CuX(pyz)_2]Y$ family $[CuCl(pyz)_2](BF_4)$ **1** and $[CuBr(pyz)_2](BF_4)$ **2** with a short monatomic connectivity between the layers by halide ions. Syntheses and crystal growth are discussed. The crystal and magnetic structures were determined by X-ray and neutron diffraction. The experimental electron density distribution is compared to the density functional theory (DFT) one. The magnetic properties were determined by superconducting quantum interference device (SQUID) and electron spin resonance (ESR) measurements and discussed in the $[Cu(pyz)_2]^{2+}$ series.

■ EXPERIMENTAL SECTION

Synthesis. The title compounds were obtained via two synthetic routes.

Method 1: $[CuCl(pyz)_2](BF_4)$, **1**, was crystallized from a solution of stoichiometric amounts of 4.9894 g of $Cu(BF_4)_2\cdot 6H_2O$ (Alfa Aesar, 98%), 0.7730 g NH_4Cl (Merck, 99.8%), and 2.3148 g of pyrazine (Acros, 99+%) in 0.5 L of water according to reaction 1. The mixture was cooled until **1** precipitated (yield 32%).

$$Cu(BF_4)_2 + NH_4Cl + 2pyz \rightarrow [CuCl(pyz)_2](BF_4) + NH_4BF_4 \tag{1}$$

Method 2: $[CuCl(pyz)_2](BF_4)$, **1**, was obtained from an aqueous solution of 1.9431 g of $CuCl_2$ (Aldrich, ≥99.995%), 2.8134 g of $Ag(BF_4)$ (Strem, 99%), and 2.3148 g of pyrazine (Acros, 99+%) according to reaction 2. First, $CuCl_2$ was dissolved in 250 mL of H_2O, and $Ag(BF_4)$ was added. After 30 min of stirring, the precipitated AgCl was filtered off. Then the pyrazine dissolved in 250 mL of water was slowly added. The mixture was cooled until precipitation occurred (yield 60%). Upon slow evaporation at 5 °C during a few weeks, dark blue crystals with a tetragonal prismatic habitus were obtained.

$$CuCl_2 + Ag(BF_4) + 2pyz \rightarrow [CuCl(pyz)_2](BF_4) + AgCl \tag{2}$$

$[CuBr(pyz)_2](BF_4)$, **2**, was synthesized according to method 2 from $CuBr_2$ (Aldrich, 99.999%).

For powder neutron diffraction measurements deuterated samples were prepared. They were synthesized from deuterated pyrazine (D_4-pyz, CIL, >98% D) and D_2O (ARMAR, 99.8% D). The samples were dried for 1 h in vacuum at room temperature.

Characterization. The thermal stability range of the compounds was determined on a Mettler Toledo TGA/SDTA851 thermo-balance. Samples of ~20 mg weight were heated by 5 K/min in corundum crucibles in a N_2 gas flow of 20 mL/min. The thermogravimetric analysis (TGA) curves are shown in Figure S1 of the Supporting Information.

Fourier transform infrared (FTIR) spectra were measured on a JASCO FT/IR-4700 spectrometer. An FTIR spectrum of **1** is shown in Figure S2 of Supporting Information.

Single-Crystal X-ray Diffraction. Crystals were mounted with grease on a glass fiber and cooled by an Oxford cryostream N_2 flow cryostat. Preliminary measurements were performed at 173(2) K up to a resolution of 0.67 Å, whereas extensive high-resolution data collections (d_{min} = 0.45 Å) were performed at 100(2) K, for $[CuCl(pyz)_2](BF_4)$, $[CuCl(D_4\text{-}pyz)_2](BF_4)$, and $[CuBr(pyz)_2](BF_4)$. All measurements were made on an Oxford Diffraction SuperNova area-detector diffractometer using mirror optics, monochromated, and Al filtered[20] microsource Mo Kα radiation (λ = 0.710 73 Å). Data reduction was performed using the CrysAlisPro program.[21] Intensities were analytically corrected for Lorentz and polarization effects and for absorption with the Gaussian method based on the crystal shape. The pyrazine H atoms were placed in positions calculated theoretically and refined using a riding model. Selected crystallographic data and structural refinement details are summarized in Table 1. Atomic positions and equivalent isotropic displacement parameters are given in Table S2 of Supporting Information.

Table 1. High-Resolution Crystal Data and Structure Refinement of $[CuCl(pyz)_2](BF_4)$ 1 and $[CuBr(pyz)_2](BF_4)$ 2 at 100 K

empirical formula	$[CuCl(pyz)_2](BF_4)$	$[CuBr(pyz)_2](BF_4)$
formula weight, g mol^{-1}	345.98	390.45
temperature, K	100(2)	100(2)
crystal system	tetragonal	tetragonal
space group	*P*4/*nbm* (125)	*P*4/*nbm* (125)
a, *b*, Å	9.74670(10)	9.75710(10)
c, Å	5.617 90(10)	5.845 00(10)
volume, Å^3	533.690(14)	556.450(15)
Z	2	2
ρ_{calc}, g cm^{-3}	2.153	2.330
μ, mm^{-1}	2.341	5.595
F(000)	342	378
2θ range, deg	5.9−105.3	5.9−91.2
index ranges	$-21 \le h \le 21$	$-19 \le h \le 19$
	$-21 \le k \le 21$	$-19 \le k \le 19$
	$-12 \le l \le 12$	$-11 \le l \le 11$
collected/independent reflections	31 788/1655	39 145/1252
R_{int}	0.017	0.027
R_σ	0.005	0.007
spherical atom refinement		
data/restraints/parameters	1655/0/32	1252/0/27
goodness-of-fit on F^2	1.145	1.115
final *R* indexes [$I \ge 2\sigma(I)$]	R_1 = 0.016	R_1 = 0.017
	wR_2 = 0.05	wR_2 = 0.04
final *R* indexes [all data]	R_1 = 0.017	R_1 = 0.022
	wR_2 = 0.05	wR_2 = 0.04
largest diff peak/hole, e Å^{-3}	0.65/−0.69	0.64/−0.52
multipole model refinement		
data/restraints/parameters	1655/5/105	1252/5/103
final *R* indexes [all data]	R_1 = 0.011	R_1 = 0.019
	wR_2 = 0.02	wR_2 = 0.02
largest diff peak/hole, e Å^{-3}	0.28/−0.25	0.33/−0.32

The conventional structural refinements were performed using SHELXL.[22] Multipole refinements with the Hansen-Coppens formalism[23] for accurate charge density determination were performed using XD2015.[24] More details on the multipolar models are given in the Supporting Information. The highest and lowest residual density peaks were 0.28 and −0.25 e Å^{-3} for **1** and 0.33 and −0.32 eÅ^{-3} for **2** using in both cases all the data. Residual density maps show only small and random discrepancies.

The d-orbital occupancies were derived with the assumption of low sp to d overlap, according to the approach suggested by Holladay, Leung, and Coppens[25] using the XDPROP module. Topological properties and integrated atomic charges were calculated using the TOPXD module.

Powder X-ray Diffraction. Powder X-ray diffraction patterns were measured on a STOE STADIP diffractometer in Debye−Scherrer geometry at room temperature. Samples were prepared on thin plastic foil. Diffraction patterns were measured with Cu Kα1 radiation (λ = 1.540 59 Å) from a focusing Ge (111) monochromator and recorded with a position-sensitive Mythen 1K detector with 0.01° resolution in 2θ.

Low-temperature X-ray diffraction patterns were measured at the powder diffraction station of the Swiss Light Source at the Paul Scherrer Institute (PSI).[26] The sample was filled in a 0.3 mm capillary and cooled in a He flow cryostat. Data were measured between 5 and 290 K at a wavelength of $\lambda = 0.564\,96$ Å. The temperature-dependent unit-cell parameters were refined with Topas Academic.[27]

Powder Neutron Diffraction. Powder diffraction patterns were measured on the cold neutron diffractometer DMC[28] of the Swiss spallation neutron source at PSI. Powder samples of 3 g of deuterated $[CuX(D_4\text{-pyz})_2](BF_4)$ with X = Cl and Br were sealed in V cans under He gas. Neutrons with wavelengths of $\lambda = 4.5040$ and 3.8040 Å were used. The samples were cooled in an ILL-type He cryostat (ILL = Institute Laue-Langevin) with a base temperature of 1.5 K.

Powder diffraction data were analyzed with the FullProf program package.[29,30]

Magnetic Measurements. Magnetic susceptibility data were recorded on a Quantum design MPMS-5XL SQUID magnetometer in the temperature range from 1.9 to 300 K and a magnetic field of 0.2 T for a crystal and deuterated powder of **1**, 0.1 T for a powder of **2**, and 0.05 T for a powder of **1**. Magnetization measurements were done at 1.9 K in fields up to 5 T. Susceptibility data were corrected for diamagnetic contributions from the sample ($-0.45\cdot10^{-6}$ cm^3/g·molar weight), the empty sample holder, and the temperature-independent paramagnetic contribution of Cu^{2+}.

ESR Spectroscopy. ESR spectra of powder and crystal samples were recorded on a Bruker E-500 spectrometer in the X-band at room temperature.

Electronic Structure Calculations. Periodic DFT calculations were performed using the software CRYSTAL14.[31] The functional B3LYP was used with basis set 86-411G(41d)[32] for the Cu and pob-TZVP[33] for all the other atoms. The theoretical electron density was analyzed with the TOPOND module of CRYSTAL14. Selected crystal dimeric/tetrameric units were calculated with Gaussian09[34] using again the B3LYP functional and the basis set 6-311G(2d,2p). More details about the dimeric/tetrameric units are given in the Supporting Information.

■ RESULTS AND DISCUSSION

$[CuCl(pyz)_2](BF_4)$, **1**, and $[CuBr(pyz)_2](BF_4)$, **2**, are isostructural and crystallize in the tetragonal space group *P*4/*nbm*, see Figure 1. Room-temperature powder diffraction pattern and Rietveld fits, see Figures S3 and S4 of Supporting Information, demonstrate the phase purity of the samples, and they perfectly agree with single-crystal data. In these structures, the Cu^{2+} ions have a distorted octahedral coordination by four N atoms from pyrazine in the tetragonal plane and by two halide anions along the *c*-axis. The Cu−N distances of 2.054 and 2.056 Å are rather close, whereas the Jahn−Teller distorted Cu−X distances increase from 2.809 (**1**) to 2.923 (**2**) Å, see Table 2. Both the pyrazine and the halide ligands act as bidentate linkers connecting Cu^{2+} ions into a 3D coordination network. The pyz rings are rotated around the Cu−N−N−Cu axis by 58.4° (**1**) and 55.0° (**2**) from the tetragonal plane. The BF_4^- anions occupy voids in the 3D network and are linked by F···H bonds to pyz molecules.

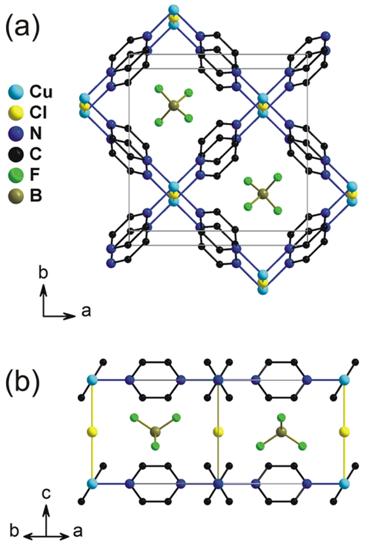

Figure 1. View onto the crystal structure of $[CuCl(pyz)_2](BF_4)$ (a) along the *c*-axis and (b) along [110]. Hydrogen atoms are omitted for clarity. The unit cell is outlined by gray lines.

Table 2. Atomic Distances (Å) and Angles (deg) of $[CuCl(pyz)_2](BF_4)$, 1, and $[CuBr(pyz)_2](BF_4)$, 2, at 100 K

	$[CuCl(pyz)_2](BF_4)$	$[CuBr(pyz)_2](BF_4)$
Cu−N (4×)	2.0544(3)	2.0559(5)
Cu−X (2×)	2.8089(1)	2.9225(1)
pyz rotation angle	58.35(2)	55.01(3)
Cu−Cu distances		
Cu−pyz−Cu (= |**a** + **b**|/2)	6.8920(1)	6.8993(1)
Cu−X−Cu (= |**c**|)	5.6179(1)	5.8450(1)

The 3D structural network explains some of the chemical properties of these compounds. They have a rather low solubility in water and rapidly precipitate as powder, which hardly redissolves. Single crystals of millimeter size and tetragonal prismatic habitus grew by slow evaporation over several weeks at 5 °C. The 3D coordination network gives rise to high thermal stability. **1** and **2** decompose in a one-step process above 240 and 227 °C, respectively, see the TG curves in Figure S1 of Supporting Information. The decomposition product is the respective monovalent copper halide CuX with X = Cl, Br, as confirmed by powder X-ray diffraction.

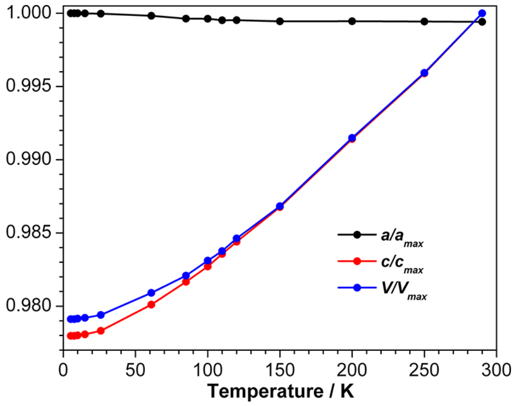

Figure 2. Temperature dependence of the reduced lattice parameters and molar volume of $[CuCl(pyz)_2](BF_4)$. The lines are a guide.

Temperature-dependent powder X-ray diffraction measurements provided information on the thermal expansion of $[CuCl(pyz)_2](BF_4)$. The relative change of lattice parameters and molar volume is shown in Figure 2, and more details are given in Table S1 of Supporting Information. The thermal lattice expansion is very anisotropic. Along the *a*-axis (= *b*) one observes even a slight contraction $\Delta a/a = -0.1\%$, whereas along the *c*-axis the lattice strongly expands by $\Delta c/c = 2.1\%$. The molar volume increases by 1.9% from 160.44(1) to 163.63(1) cm^3/mol between 5 and 290 K. These results demonstrate the extraordinary rigidity of the $[Cu(pyz)_2]^{2+}$

Table 3. Structural and Magnetic Parameters of Compounds with Tetragonal $[Cu(pyz)_2]^{2+}$ Layers[a]

			distance (Å)		Cu−Cu distance (Å)			$J_{\parallel}$	T_N	
No.	compound	space group	Cu−N	Cu−X	Cu−pyz−Cu	Cu−X−Cu	pyz rot. angle (deg)	(K)	(K)	ref
1	$[Cu(HF_2)(pyz)_2](SbF_6)$	*P*4/*nmm*	2.048	2.338	6.876	6.97	81.4	13.4	4.3	[18][b]
2	$[Cu(HF_2)(pyz)_2](TaF_6)$	*P*4/*mmm*	2.047	2.367	6.862	7.027	90.0	13.1	4.2	[19][c]
3	$[Cu(HF_2)(pyz)_2](AsF_6)$	*P*4/*mmm*	2.046	2.333	6.865	6.950	90.0	12.8	4.3	[4]
4	$[Cu(HF_2)(pyz)_2](PF_6)$	*P*4/*mmm*	2.041	2.312	6.854	6.893	90.0	12.4	4.3	[4, 35]
5	$[Cu(NO_3)(pyz)_2](PF_6)$	*I*4/*mcm*	2.042	2.413	6.866	7.003	61.4	10.8	2.0	[16, 36][d]
6	$[CuCl(pyz)_2](BF_4)$, **1**	*P*4/*nbm*	2.053	2.865	6.895	5.731	58.8	9.4	3.9	this work
7	$[CuBr(pyz)_2](BF_4)$, **2**	*P*4/*nbm*	2.052	2.963	6.894	5.926	55.4	8.9	3.8	this work
8	$[Cu(NO_2)(pyz)_2](ClO_4)$	*P*4/*nbm*	2.049	2.285	6.877	6.646	59.8	8.9	N/A	[37]
9	$[Cu(HF_2)(pyz)_2](ClO_4)$	*P*4/*nbm*	2.040	2.228	6.863	6.689	64.2	7.3	1.9	[4]
10	$[Cu(HF_2)(pyz)_2](BF_4)$	*P*4/*nbm*	2.039	2.208	6.852	6.619	59.4	6.3	1.5	[4, 17, 38]

[a] The pyz rotation angle is the deviation from the tetragonal layer. All data at room temperature, except for No. 5 at 163 K. [b] [4] reports space group *P*4/*mmm* and 90° pyz rotation angle at room temperature. At 90 K, the pyz rotation angle is 79.1°. [c] At 90 K, the space group is *P*4/*nmm* with a pyz rotation angle of 79.5°. [d] The structure is highly disordered.

layers and the softness of the Jahn−Teller distorted Cu−X−Cu bonds within the 3D coordination network.

The crystal structures of **1** and **2** are closely related to $[Cu(HF_2)(pyz)_2]Y$ with Y = ClO_4^-, PF_6^-, SbF_6^-, AsF_6^-, or TaF_6, see Table 3. All these tetragonal compounds contain $[Cu(pyz)_2]^{2+}$ layers as their characteristic structural feature. Further related compounds with distorted $[Cu(pyz)_2]^{2+}$ square nets, for example, $[Cu(ClO4)_2(pyz)_2]$ and $[Cu(pyz)_2(NO_3)]$-$NO_3 \cdot H_2O$, are summarized in Table S3 of Supporting Information. In $[Cu(pyz)]^{2+}$ compounds, the angle between the tetragonal plane and the pyz ring is close to 90° for bigger octahedral Y anions, or close to 60° for smaller tetrahedral anions; the only exception is Y = PF_6^- which gives both, depending on the interlayer linker, see Table 3. We note, however, when low-*T* measurements are available, all structures have a pyrazine rotation angle smaller than 90°. Some structures at room temperature have been refined in *P*4/*mmm*,[4,19,34] therefore with pyz necessarily orthogonal to the tetragonal layer. However, a careful inspection of atomic displacement parameters of pyz C atoms in these structures reveals that these are compatible with a disorder between two orientations of the pyrazine ring, and therefore the reported 90° angles are deceptive.

In the $[CuX(pyz)_2](BF_4)$ compounds **1** and **2**, the layers are linked by monatomic halide ligands, which is unprecedented for the $[Cu(pyz)]^{2+}$ structural family. For all other compounds, the connection occurs via polyatomic anions, such as FHF^-, NO_2^-, or NO_3^-, as well as BF_4^- and ClO_4^- for the distorted square nets. Accordingly, **1** and **2** show the by far shortest interlayer Cu−X−Cu distances, which are significantly shorter than the intralayer Cu−pyz−Cu distances, see Table 2.

The Cu−ligand distances in $[CuX(pyz)_2](BF_4)$ indicate that the elongated Jahn−Teller axis is located parallel to the *c*-axis, and therefore the unpaired electron of the $d_{x^2-y^2}$ orbital localized in the *ab* plane. As local coordinate system for the Cu^{2+} ion, we adopt $x = a + b$, $y = a - b$, and $z = c$. Therefore, the magnetic interactions predominantly occur within the $[Cu(pyz)_2]^{2+}$ layers of the *ab* plane, resulting in a quasi 2D magnetic network, despite the 3D nature of the coordination network and the shorter interlayer Cu−X−Cu distances.

If the Cu−pyz direction was instead Jahn−Teller distorted, the Cu−N distances would be ∼2.40 Å, see, for example ref 14, which is distinctly longer than the observed distances reported in Table 2.

From high-resolution single-crystal X-ray diffraction experiments at 100 K and periodic DFT calculations the electron density distribution in both compounds was determined. The coefficients of the experimental multipolar refinement were converted into occupancies of the d-orbitals.[25] In agreement with periodic DFT calculations, the electron population of the $d_{x^2-y^2}$ orbital is distinctly smaller than for all other d orbitals, see Table 4. This result confirms that $d_{x^2-y^2}$ is, in a first approximation, the single-occupied, magnetic orbital. It is generally observed that the experimental multipole refinements exceed the occupation of 2.0 for fully occupied orbitals, see, for example, ref 39. These parameters were freely refined without a constraint and represent d-shaped electron density functions, not directly 3d-orbitals. A comparison with multipole refinements fitted to theoretical data (DFT) is very useful, see Table 4, indicating a good agreement between theory and experiments, when the same multipolar expansion is applied. The experimental deformation density maps clearly confirm the charge depletion of the Cu^{2+} ion along the *x* and *y* directions in the local coordinate system, see Figure 3.

Table 4. d-Electron Populations from Experimental Multipolar Refinements (exp MM), Multipolar Refinements of Theoretical Calculations (calc MM), and Periodic DFT Calculations (calc)

	$d_{x^2-y^2}$	d_{xz}	d_{xy}	d_{yz}	d_{z^2}
		$[CuCl(pyz)_2](BF_4)$, **1**			
exp MM	1.644(3)	2.102(2)	1.996(3)	2.102(2)	2.196(4)
calc MM	1.609	2.120	2.114	2.120	2.123
calc	1.393	1.981	1.977	1.981	1.986
		$[CuBr(pyz)_2](BF_4)$, **2**			
exp MM	1.631(5)	2.099(4)	2.091(5)	2.099(4)	2.068(6)
calc MM	1.610	2.128	2.088	2.128	2.135
calc	1.393	1.980	1.978	1.980	1.985

The topological analysis of the experimental and theoretical electron densities, through quantum theory of atoms in molecules (QTAIM),[40] enables addressing the main bonding features in the two structures, see Table S4 of Supporting Information. In particular, we focus the attention on bonds to Cu and electron sharing, including delocalization between atoms not directly connected by a bond path. The electron delocalization indices cannot be derived from the experimental

DOI: 10.1021/acs.inorgchem.7b03150
Inorg. Chem. XXXX, XXX, XXX−XXX

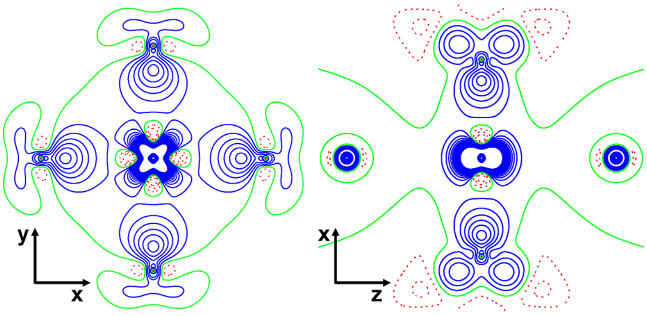

Figure 3. Static deformation electron density maps of **1**. The *xy* and *x*−*z* planes (in the local Cu^{2+} coordinate system) are depicted. Blue and red contours (0.2 e/Å^3), respectively, represent the excess and depletion of electron density with respect to the spherical atom distribution. The green contour is the zero level.

electron density, but they are computed from gas-phase calculations on a dimeric $[Cu_2X_4(pyz)_7]$ unit.

In general, the two compounds show very similar features, both in the experimental and the theoretical analysis. The electron density calculated at the bond critical points of Cu−X bonds is ca. 1/3 that of Cu−N bonds. Similarly, the electron delocalization indices of Cu−X bonds are ca. 1/2 of Cu−N bonds. This mainly reflects the Jahn−Teller distortion and the lower (though not-negligible) electron sharing occurring along this coordination direction. The 1,3 C−C and C−N interactions in the pyrazine ring have an electron delocalization of ca. 0.1 electron pairs due to the large resonance within the aromatic ligand. Of course, the 1,2 interactions have a much larger delocalization of ca. 1.3 electron pairs. Instead, the 1,3 Cu−C interaction is much weaker (<0.02 electron pairs). This confirms the previous suggestion that a π driven Cu−Cu magnetic exchange through the pyrazine is not favorable; this would be possible only through a significant Cu−C exchange, which does not occur, see, for example, the discussion in ref 39. The Cu−N interaction cannot provide any contribution to a π driven Cu−Cu magnetic exchange, because the atomic orbitals p_z of N and $d_{x^2-y^2}$ of Cu are necessarily orthogonal to each other. Accordingly, the large Cu−N exchange can only contribute via σ-type mechanism to the Cu−Cu exchange. This is confirmed by the calculated spin density distribution for the dimer, see Figure 4.

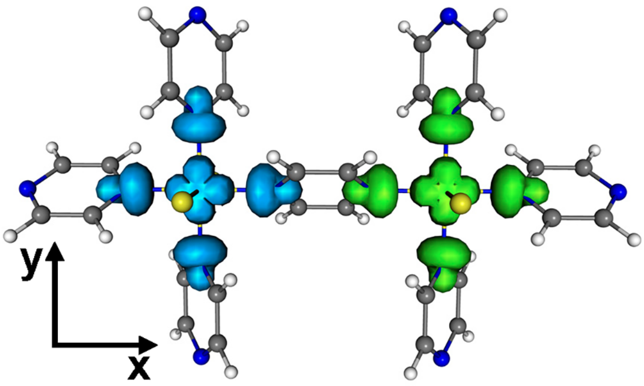

Figure 4. Calculated spin density distribution imposes an antiferromagnetic coupling in the $[Cu_2Cl_4(pyz)_7]$ dimer. Cyan and green surfaces represent excess and defect of α spin density at values ±0.013 eÅ^{-3}.

The atomic charges, obtained from the QTAIM partitioning of the experimental and theoretical electron densities of the crystals or the theoretical electron density of the dimeric units, are reported in Table S5 of Supporting Information. In all cases, the actual charge of Cu is smaller than the formal oxidation state, and the pyrazine is slightly positive, indicating that the σ-donation mechanism is dominating. The halide linkers have a negative charge, though significantly reduced from the formal −1.0, especially for the experimental multipolar model. The BF_4 anion has a charge of ca. −1.0 (with highly positive B and negative F atoms), indicating rather perfect ionic interaction between the cationic $[CuX(pyz)_2]^+$ network and the interstitial BF_4^- anions.

The magnetic structures of **1** and **2** were determined from deuterated powder samples by neutron diffraction in the temperature range from 1.5 to 15 K. A neutron diffraction pattern of $[CuBr(D_4\text{-}pyz)_2](BF_4)$ measured on DMC with λ = 4.5040 Å at 1.5 K is shown in Figure 5a, and the magnetic structure is shown in Figure 5b. The agreement factors for the Rietveld refinement are R_p = 2.9%, R_{wp} = 4.3%, R_{exp} = 0.8%,

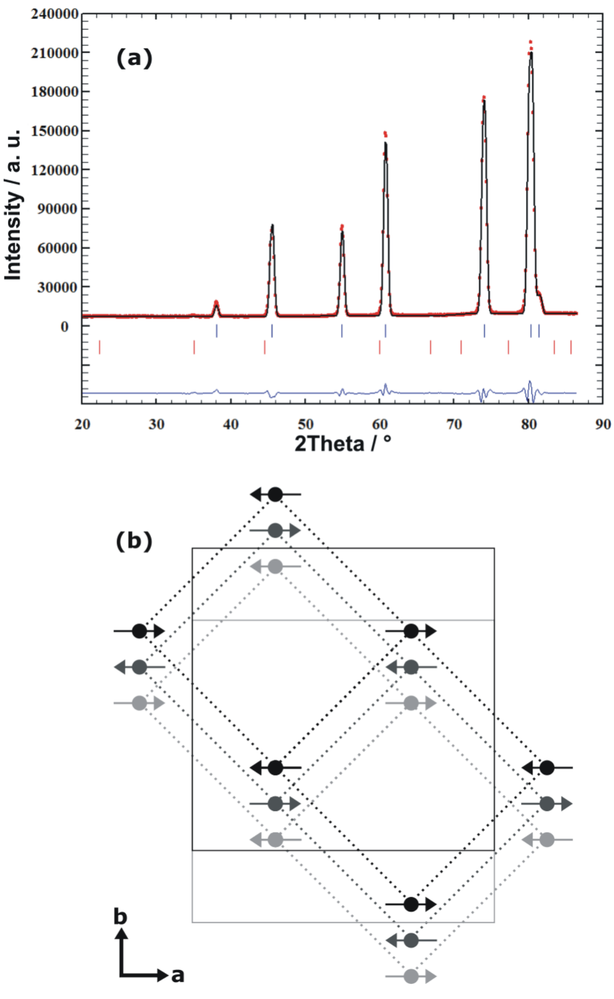

Figure 5. (a) Powder neutron diffraction pattern of $[CuBr(D_4\text{-}pyz)_2](BF_4)$ at 1.5 K (DMC, λ = 4.5040 Å). The graph shows the diffraction pattern (red dots), the Rietveld refinement (black line), the nuclear (blue ticks) and magnetic (red ticks) Bragg positions, and the difference curve (blue line). (b) Magnetic structure with $\boldsymbol{k}$ = (0, 0, 0.5) in a perspective view along the *c*-axis. Full lines denote the unit cell, and dashed lines indicate the Cu^{2+} ion square nets at heights of *z*/*c* = 0, 1, and 2.

R_{Bragg} = 1.7%, and R_{mag} = 48.6%. A neutron diffraction pattern of $[CuCl(D_4\text{-pyz})_2](BF_4)$ and the low-angle diffraction patterns with the magnetic contributions are shown in Figure S6 of Supporting Information. Because of the long wavelength the number of accessible nuclear Bragg peaks was very limited. Therefore, the atomic parameters were fixed to values obtained from 15 K neutron data measured with λ = 3.8040 Å. When cooled from 15 to 1.5 K, weak additional magnetic Bragg peaks appeared below T_N = 3.9(1) K for **1** and 3.8(1) K for **2**, which originate from long-range (3D) antiferromagnetic order of the Cu^{2+} spins. For both compounds, the magnetic Bragg peaks are indexed by the propagation vector $\boldsymbol{k}$ = (0, 0, 0.5); it indicates that the magnetic unit cell is doubled along the *c*-axis with respect to the crystallographic unit cell. Accordingly, the magnetic unit cell contains four Cu^{2+} ions, see Table 5. The best fit of the intensities was obtained for a magnetic structure with ordered moments in the tetragonal plane and AFM coupling both in the *ab* plane and along the *c*-axis, see Figure 5b. Since the Cu−ligand−Cu angles are 180° along all magnetic exchange paths of the $[CuX(pyz)_2]^+$ framework the observed AFM coupling agrees with theoretical expectations. At 1.5 K the ordered magnetic moments amount to μ_x = 0.76(8) μ_B/Cu^{2+} for **1** and 0.6(1) μ_B/Cu^{2+} for **2**. For uniaxial symmetry, as it is the case for the tetragonal title compounds, neutron powder diffraction data reveal the magnitude of the ordered magnetic moment, its angle with the *c*-axis, and the relative phase between the magnetic ions. The absolute orientation of the ordered moment within the *ab* plane cannot be determined. Therefore, the calculations were done for magnetic moments aligned along the *a*-axis.

Table 5. Cu Atomic Positions in the Magnetic Unit Cell with $\boldsymbol{k}$ = (0, 0, 0.5) and Ordered Moments[a] $\boldsymbol{\mu_x}$ of $[CuCl(pyz)_2](BF_4)$, 1, and $[CuBr(pyz)_2](BF_4)$, 2, at 1.5 K

	x/a	y/b	z/c	μ_x/μ_B, **1**	μ_x/μ_B, **2**
Cu1	0.25	0.25	0	0.76(8)	0.6(1)
Cu2	0.75	0.75	0	−0.76	−0.6
Cu3	0.25	0.25	1	−0.76	−0.6
Cu4	0.75	0.75	1	0.76	0.6

[a] $\mu_y = \mu_z = 0\ \mu_B$

For $[CuCl(D_4\text{-pyz})_2](BF_4)$ a *g*-value of 2.132 was determined from ESR measurements, see below. Accordingly, $g{\cdot}S$ = 1.07 μ_B/Cu^{2+} is expected for a fully ordered moment. The observed value of 0.76 μ_B/Cu^{2+} is reduced but in good agreement with values of other Cu^{2+} compounds, for example, $Cu(DCO_2)_2{\cdot}4D_2O$,[41,42] indicating quantum fluctuations below T_N. The magnetic contributions to the neutron diffraction pattern in Figure 5 are rather tiny. This is a result of the small S = 1/2 spin of Cu^{2+}, since the magnetic intensity is proportional to the square of the ordered moments. The tiny intensity manifests in a large R_{mag} = 48.6% value for the magnetic refinement. Nevertheless, the AFM magnetic structure was clearly determined as the best solution with respect to magnetic peak positions and intensities. Calculations for all other spin orientations resulted in R_{mag} > 85% values.

The temperature dependence of the integrated intensity of the strongest magnetic peak (−101) at 35.7° 2θ is shown in Figure 6. A fit to the power law in eq 3 yields the Néel temperatures T_N = 3.9(1) K and 3.8(1) K for the chloride and bromide, respectively. The critical exponent β = 0.23 for a 2D Heisenberg magnet was kept fixed in the fits due to the limited number of data points. The determined Néel temperatures are in good agreement with magnetic susceptibility measurements below.

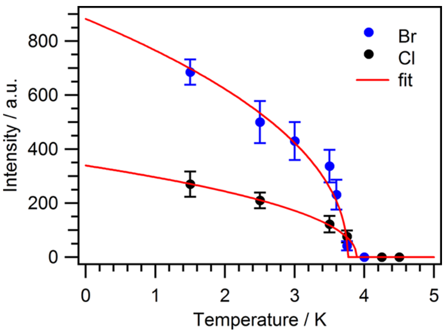

Figure 6. Temperature dependence of the integrated intensity of the (−101) magnetic Bragg peak of **1** (black dots) and **2** (blue dots). Fits to a power law (red lines) result in T_N = 3.9(1) K for **1** and T_N = 3.8(1) K for **2**.

$$I = I_0(1 - T/T_N)^{2\beta} \tag{3}$$

The Cu^{2+} *g*-values and their anisotropy were determined from X-band ESR spectra at room temperature, see Figure 7.

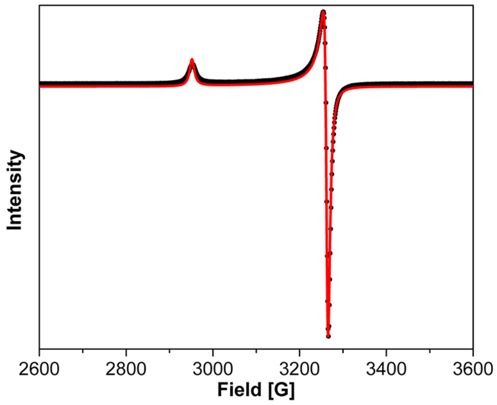

Figure 7. Experimental (black dots) and simulated (red line) X-band ESR spectrum of $[CuCl(D_4\text{-pyz})_2](BF_4)$ powder. The fit results in g_x = 2.060(1) and g_z = 2.275(1).

For nondeuterated and deuterated $[CuCl(pyz)_2](BF_4)$ powder samples values of g_x = 2.061(1), g_z = 2.276(1), and g_x = 2.060(1), g_z = 2.275(1) were obtained, respectively. Within error limits, the values of the H and D samples are equal. They result in an average g = 2.132(1) for **1**. For the bromide g_x = 2.057(1) and g_z = 2.272(1) were determined with an average g = 2.129(1). The ESR spectra are in perfect agreement with the crystal structure exhibiting a single Cu^{2+} site of axial symmetry, see Table S2 of Supporting Information. Similar *g* values were reported for related $[Cu(pyz)_2]^{2+}$ compounds.[19,34,37,43,44]

The anisotropy of the Cu^{2+} *g*-value was measured for a nondeuterated single crystal of **1** at room temperature. The tetragonal prismatic crystal had almost equal edges of 1 mm length. Its orientation was verified by X-ray diffraction. Data for a rotation around the *b*-axis are shown in Figure 8. A sine fit results in values of g_x = 2.058(1) and g_z = 2.274(1). A second data set (not shown here) for the rotation around the *c*-axis resulted in an isotropic value of g_x = 2.060(1). These single-crystal values are in good agreement with powder data. They

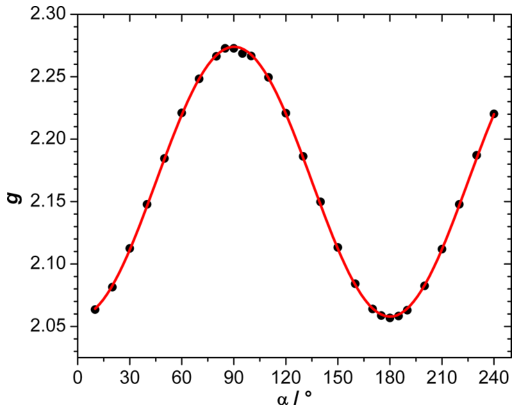

Figure 8. Angular dependence α of the g-value (black dots) of **1** in the ac plane from single-crystal ESR spectra. A sine fit (red line) results in values of $g_x = 2.058(1)$ and $g_z = 2.274(1)$.

confirm the axial anisotropy of the g tensor in $[\mathrm{CuX(pyz)_2}](\mathrm{BF_4})$ and the $g_x < g_z$ assignment.

The magnetic susceptibility χ and the $\chi{\cdot}T$ product versus temperature are shown in Figures 9 and S5 of Supporting Information, respectively. At 300 K the $\chi{\cdot}T$ values of 0.4139 $\mathrm{cm^3}$ K/mol for **1** and 0.4123 $\mathrm{cm^3}$ K/mol for **2** were determined. They are in good agreement with the expectation value of $\chi{\cdot}T = 0.125\,05{\cdot}g^2{\cdot}S{\cdot}(S+1) = 0.4255$ $\mathrm{cm^3}$ K/mol with $S = 1/2$ and $g = 2.132$ from ESR. The $\chi{\cdot}T$ values decrease with temperature and show a steep decline below 50 K due to antiferromagnetic interactions.

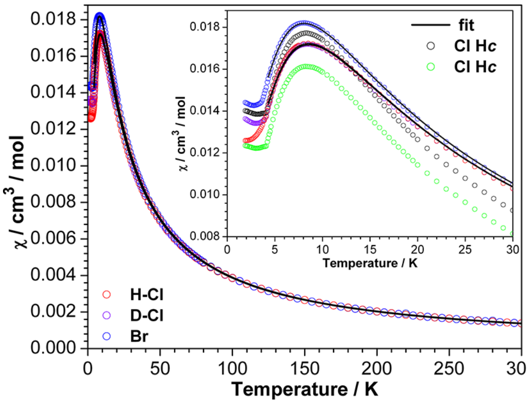

Figure 9. Temperature dependence of the magnetic susceptibility χ for powder samples of nondeuterated **1** (red ○), deuterated **1** (purple ○), and **2** (blue ○). (inset) Magnification of the low-temperature part, where single-crystal data of **1** for $H \| c$ (green ○) and $H \perp c$ (black ○) are added. Fits to a 2D Heisenberg model (black lines) are shown for powder samples of **1** and **2** between 4.3 and 300 K.

The magnetic susceptibility χ shows a broad maximum at ∼8 K, see Figure 9. The maximum occurs due to predominantly 2D AFM interactions in the $[\mathrm{Cu(pyz)_2}]^{2+}$ planes. According to $J_{\|} = 1.07{\cdot}T_{\max}$ an in-plane coupling parameter of $J_{\|} \approx 9$ K can be estimated for a 2D Heisenberg system. Data were fitted to a 2D spin 1/2 Heisenberg model between 4.3 and 300 K, see eq 4.[45] The model includes a small percentage p of paramagnetic impurities with coefficients N_i and D_i from ref 45.

$$\chi = \frac{C}{T}\left[1 + \frac{\sum_{i=1}^{5} N_i\left(\frac{J}{k_B T}\right)^i}{1 + \sum_{i=1}^{5} D_i\left(\frac{J}{k_B T}\right)^i}\right](1-p) + \frac{pC}{T} \tag{4}$$

The fit results in $J_{\|} = 9.4(1)$ K for **1** and 8.9(1) K for **2**, in good agreement with the estimation from $T_{\max}$. The paramagnetic impurities are 1.0(1) % for **1** and 1.3(1) % for **2**. The expression $g{\cdot}B_s/J_{\|} \approx 6.03\ T$ [4] results in an estimate for the saturation field along the c-axis of $B_s \approx 25$ T for **1** and 24 T for **2**. The interplane coupling $J_{\perp}$ is determined by T_N and $J_{\|}$. For a quasi-2D Heisenberg antiferromagnet the values are related by eq 5

$$|J_{\perp}| = J e^{b - 4\pi\rho_s/T_N} \tag{5}$$

with $b = 2.43$ and the spin stiffness $\rho_s = 0.183\ J$ for an $S = 1/2$ system.[46] This results in $|J_{\perp}| = 0.31(6)$ K for **1** and 0.52(9) K for **2**.

Weak magnetic interactions between the $[\mathrm{Cu(pyz)_2}]^{2+}$ layers give rise to 3D order at lower temperature, as proven by neutron diffraction above. The 3D order appears as a kink in the magnetic susceptibility below 4 K, see the inset in Figure 9. The ratios of $T_N/J_{\|} = 0.41$ for **1** and 0.43 for **2** indicate significant interactions between the layers. As for the ESR data, the magnetic susceptibility data for nondeuterated and deuterated samples of **1** were equal within error limits. Only small variations in the paramagnetic impurities were observed between the different samples.

Single-crystal susceptibility data of $[\mathrm{CuCl(pyz)_2}](\mathrm{BF_4})$ for H$\|c$ and H$\perp c$ coincide from 300 to 190 K (data not shown here). Toward lower temperature, see the inset in Figure 9, an anisotropy is observed with higher χ values for H$\perp c$, which is in agreement with the magnetic structure, see Figure 5b, and ordered moments in the ab plane.

Magnetization measurements of **1** and **2** at 1.9 K are shown in Figure 10. The magnetization increases approximately linearly with the magnetic field up to ∼1 T. For higher fields the curves show an upturn and rise faster than linear. Such behavior is typical for low-dimensional AFM coupled $\mathrm{Cu^{2+}}$ compounds with a low-spin (singlet) ground state.[4,18,47−49] Spins gradually align with increasing magnetic field resulting in the upturn of the magnetization. The observed value of 734 $\mathrm{cm^3}$ G/mol for **1** at 5 T is far from saturation, where $M = N{\cdot}\mu_B{\cdot}g{\cdot}S = 5954$ $\mathrm{cm^3}$ G/mol is expected for $S = 1/2$ and $g = 2.132$.

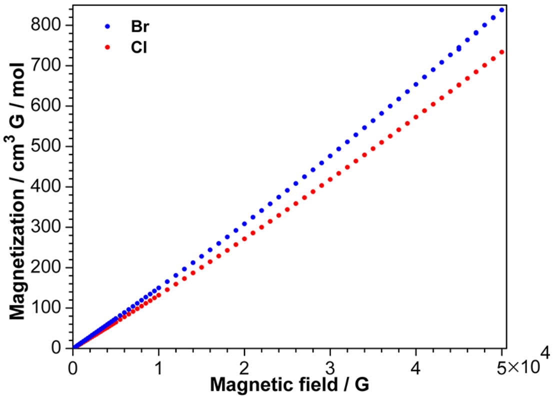

Figure 10. Magnetization of powder samples of **1** (red) and **2** (blue) at 1.9 K.

The low experimental value at 5 T is in agreement with the much higher estimated saturation field of $B_s \approx 28$ T from the 2D Heisenberg model. A slightly higher magnetization value of 838 cm^3 G/mol is observed for **2** at 5 T. It is in agreement with the smaller $J_{\|} = 8.9$ K for the bromide compared to $J_{\|} = 9.4$ K for the chloride.

The aim of the present study is to establish magneto-structural correlations in the $[Cu(pyz)_2]^{2+}$ series by adding the compounds $[CuX(pyz)_2](BF_4)$, where X = Cl and Br, with distinctly shorter Cu−X−Cu distances, see Table 3. For all compounds the Cu−pyz−Cu distances are located in a very narrow range from 6.852 to 6.895 Å. Therefore, the Cu−pyz−Cu distances do not significantly correlate with the magnetic coupling parameters represented by $J_{\|}$ (2D) and T_N (3D). In contrast, the pyz rotation angle is quite variable. For longer Cu−X−Cu distances, an increase of the pyz rotation angle is expected to reduce the steric hindrance of pyz ligands in the tetragonal plane. Although this is not valid for **1** and **2**, where the Cu−X−Cu distance is ∼0.2 Å longer in **2**, the pyz rotation angle decreases by more than 3°. In Table 3, the pyrazine rotation angle ranges from ∼55° to 90°. As discussed above, the perfectly vertical pyrazines are likely affected by disorder over two conformations. Again no significant correlation is found with the magnetic coupling: for example, in the three BF_4^- salts the pyrazine rotation angle is 55.4°, 58.8°, and 59.4° for X = Br, Cl, and HF_2, respectively, but $J_{\|}$ and T_N for the chloride and bromide are much higher than for HF_2^-. This lack of correlation agrees well with the topological analysis of the electron density, which reveals that the Cu−N exchange is predominantly σ-type and independent from the pyz rotation angle. Compound numbers **1**−**4** and **9**−**10** from Table 3 contain the same $[Cu(HF2)(pyz)_2]^+$ 3D coordination network. Noteworthy, the magnetic interactions in compounds **9** and **10** are distinctly weaker than for **1**−**4**, despite shorter Cu−X−Cu distances. The contacts between pyz and the interstitial anions have an important influence on the pyz rotation angle, too, and break a clear correlation with the Cu−X−Cu distance. Such observations are not rationalized by present models and ask for further investigation. Present theoretical modeling qualitatively explains the magnetic interactions and their dimensionality.

As a result of this multiparameter space, it appears that magneto-structural correlations can be established in narrow subsections of the $[Cu(pyz)_2]^{2+}$ family, only. For $[CuX(pyz)_2](BF_4)$ with X = Cl, Br, and (HF_2), cf. numbers **6**, **7**, and **10** in Table 3, $J_{\|}$ and T_N are displayed versus the Cu−X−Cu distance in Figure 11. Both $J_{\|}$ and T_N decrease with increasing Cu−X−Cu distance. The substitution of Y = BF_4^- by ClO_4^- (no. **9**) or X = HF_2^- by NO_2^- (no. **8**) increases $J_{\|}$, and the correlation is already broken by these small variations. These results call for further measurements and calculations of structural and magnetic properties under pressure that we are currently undertaking in our laboratories. Only the study of the same compound under various external parameters will disentangle the correlation among variables.

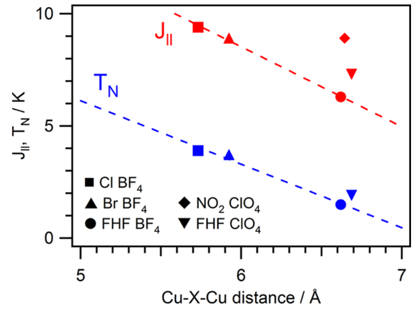

Figure 11. Correlation of $J_{\|}$ and T_N with the Cu−X−Cu distance for $[CuX(pyz)_2]Y$ compounds **6**−**10** in Table 3. The dashed lines represent linear fits for compounds with Y = BF_4^-.

■ CONCLUSIONS

Two Cu^{2+} coordination polymers $[CuX(pyz)_2](BF_4)$ with X = Cl and Br were synthesized, and single crystals were grown by controlled evaporation from aqueous solution. The isostructural tetragonal compounds consist of $[Cu(pyz)_2]^{2+}$ layers linked by halide anions X^- into a $[CuX(pyz)_2]^+$ 3D coordination network. The charge is compensated by interstitial BF_4^- anions. The monatomic halide linkage is unique among the reported $[Cu(pyz)_2]^{2+}$ compounds and result in distinctly shorter interlayer distances. The 3D coordination network gives rise to low solubility and high thermal stability. Temperature-dependent diffraction measurements revealed a pronounced structural anisotropy with rigid Cu−pyz−Cu and much softer Cu−X−Cu linkage. The shorter Cu−N and longer Cu−X bonds of the octahedral Cu^{2+} coordination indicate that the $d_{x^2-y^2}$ magnetic orbital is located in the tetragonal plane. Experimentally and theoretically derived d-orbital occupancies clearly confirm the location of the $d_{x^2-y^2}$ orbital in the *ab* plane. These materials are very important for their magnetic properties, which were characterized by neutron diffraction, magnetic susceptibility, and ESR measurements. The Cu^{2+} *g*-tensor is close to isotropic with a 10% larger g_z value at room temperature. The χ versus T curves show a broad maximum below 10 K characteristic for a 2D Heisenberg antiferromagnet. The intralayer interactions $J_{\|}$ are much stronger than magnetic interactions between the $[Cu(pyz)_2]^{2+}$ layers. Below 4 K 3D antiferromagnetic order sets in, and moments are localized in the tetragonal plane. Some open questions remain concerning the correlation of structural and magnetic properties in $[CuX(pyz)_2]Y$ compounds, which may depend on multiple parameters. The rigidity of the Cu−pyz−Cu linkage implies no correlation with $J_{\|}$ and T_N. On the contrary, the rotation of pyrazine about the Cu−N axis is quite variable and strongly depends on Y anions. However, the σ-type Cu−N exchange mechanism is necessarily independent of the pyz rotation angle. The electronic polarizability of the X linker appears less important; otherwise, a higher T_N would be expected for the bromide. Magneto-structural correlations may be drawn for narrow subsections only, as discussed for $[CuX(pyz)_2](BF_4)$ with X = Cl, Br, and HF_2. This fosters further investigations that are currently in due course in our laboratories. In particular, given the soft nature of the Cu−X−Cu interlayer connection, we expect a significant increase of the ratio between magnetic interactions $J_{\perp}/J_{\|}$ upon application of isotropic external pressure. Moreover, further chemical variations of ligands and counteranions will provide a wider data basis, which is required for more systematic analyses of correlations between structural features and magnetic exchange.

■ ASSOCIATED CONTENT

Ⓢ Supporting Information

The Supporting Information is available free of charge on the ACS Publications website at DOI: 10.1021/acs.inorgchem.7b03150.

TG curves, FTIR spectrum, powder X-ray diffraction data at RT, 5 K, and neutron diffraction data at 1.5 K, temperature-dependent lattice parameters, atomic positions and displacement parameters from single-crystal data, Table of compounds with distorted $[Cu(pyz)_2]^{2+}$ layers, details on multipole model refinements, bond critical properties, and atomic charges, ESR spectrum, and magnetic susceptibility χT versus T (PDF)

Accession Codes

CCDC 1487418−1487419 contain the supplementary crystallographic data for this paper. These data can be obtained free of charge via www.ccdc.cam.ac.uk/data_request/cif, or by emailing data_request@ccdc.cam.ac.uk, or by contacting The Cambridge Crystallographic Data Centre, 12 Union Road, Cambridge CB2 1EZ, UK; fax: +44 1223 336033.

■ AUTHOR INFORMATION

Corresponding Authors

*E-mail: piero.macchi@dcb.unibe.ch. (P.M.)
*E-mail: christian.rueegg@psi.ch. (Ch.R.)
*E-mail: karl.kraemer@dcb.unibe.ch. (K.W.K.)

ORCID

Mariusz Kubus: 0000-0002-1764-0376
Arianna Lanza: 0000-0002-7820-907X
Nicola Casati: 0000-0002-4206-9239
Karl W. Krämer: 0000-0001-5524-7703

Notes

The authors declare no competing financial interest.

■ ACKNOWLEDGMENTS

Part of this work is based on experiments performed at the Swiss spallation neutron source (SINQ) and the Swiss Light Source (SLS), Paul Scherrer Institute (PSI), Villigen, Switzerland. M.K. and B.W. acknowledge funding from the European Community's Seventh Framework Program (FP7/2007-2013) under Grant No. 290605 (PSIFELLOW/COFUND). The research leading to these results has received funding from the Swiss National Science Foundation under Grant Nos. 200020_150257 and 200020_160157.

■ REFERENCES

(1) Vaknin, D.; Sinha, S. K.; Moncton, D. E.; Johnston, D. C.; Newsam, J. M.; Safinya, C. R.; King, H. E. Antiferromagnetism in La_2CuO_{4-y}. *Phys. Rev. Lett.* **1987**, *58*, 2802−2805.

(2) Tranquada, J.; Cox, D.; Kunnmann, W.; Moudden, H.; Shirane, G.; Suenaga, M.; Zolliker, P.; Vaknin, D.; Sinha, S.; Alvarez, M.; Jacobson, A.; Johnston, D. Neutron-Diffraction Determination of Antiferromagnetic Structure of Cu Ions in $YBa_2Cu_3O_{6+x}$ with x = 0.0 and 0.15. *Phys. Rev. Lett.* **1988**, *60*, 156−159.

(3) Bednorz, J. G.; Müller, K. A. Possible high T_c superconductivity in the Ba−La−Cu−O system. *Z. Phys. B: Condens. Matter* **1986**, *64*, 189−193.

(4) Goddard, P. A.; Singleton, J.; Sengupta, P.; McDonald, R. D.; Lancaster, T.; Blundell, S. J.; Pratt, F. L.; Cox, S.; Harrison, N.; Manson, J. L.; Southerland, H. I.; Schlueter, J. A. Experimentally determining the exchange parameters of quasi-two-dimensional Heisenberg magnets. *New J. Phys.* **2008**, *10*, 083025.

(5) Christensen, N. B.; Rønnow, H. M.; McMorrow, D. F.; Harrison, A.; Perring, T. G.; Enderle, M.; Coldea, R.; Regnault, L. P.; Aeppli, G. Quantum dynamics and entanglement of spins on a square lattice. *Proc. Natl. Acad. Sci. U. S. A.* **2007**, *104*, 15264−15269.

(6) Dalla Piazza, B.; Mourigal, M.; Christensen, N. B.; Nilsen, G. J.; Tregenna-Piggott, P.; Perring, T. G.; Enderle, M.; McMorrow, D. F.; Ivanov, D. A.; Ronnow, H. M. Fractional excitations in the square-lattice quantum antiferromagnet. *Nat. Phys.* **2015**, *11*, 62−68.

(7) Carlin, R. L. *Magnetochemistry;* Springer: Berlin, Germany, 1986.

(8) Day, P.; Underhill, A. E. *Metal-Organic and Organic Molecular Magnets;* The Royal Society of Chemistry: London, UK, 1999.

(9) Bartolomé, J.; Luis, F.; Fernández, J. F. *Molecular Magnets Physics and Applications;* Springer-Verlag: Berlin, Germany, 2014.

(10) Hong, M.; Chen, L. *Design and Construction of Coordination Polymers;* Wiley, Inc.: Hoboken, NJ, 2009.

(11) Turnbull, M. M.; Sugimoto, T.; Thompson, L. K. *Molecule-Based Magnetic Materials;* American Chemical Society: Washington, DC, 1996.

(12) Willett, R. D.; Landee, C.; Swank, D. D. Magnetic susceptibility of $CuCl_2 \cdot TMSO$, a ferromagnetic spin 1/2 linear chain. *J. Appl. Phys.* **1978**, *49*, 1329−1330.

(13) Manson, J. L.; Conner, M. M.; Schlueter, J. A.; Mcconnell, A. C.; Southerland, H. I.; Malfant, I.; Lancaster, T.; Blundell, S. J.; Brooks, M. L.; Pratt, F. L.; Singleton, J.; Mcdonald, R. D.; Lee, C.; Whangbo, M. Experimental and Theoretical Characterization of the Magnetic Properties of $CuF_2(H_2O)_2(pyz)$ (pyz = pyrazine): A Two-Dimensional Quantum Magnet Arising from Supersuperexchange Interactions through Hydrogen Bonded Paths. *Chem. Mater.* **2008**, *20*, 7408−7416.

(14) Lanza, A.; Fiolka, C.; Fisch, M.; Casati, N.; Skoulatos, M.; Rüegg, C.; Krämer, K. W.; Macchi, P. New magnetic frameworks of $[(CuF_2(H_2O)_2)_x(pyz)]$. *Chem. Commun.* **2014**, *50*, 14504−14507.

(15) Nath, R.; Padmanabhan, M.; Baby, S.; Thirumurugan, A.; Tsirlin, A. A.; et al. Quasi-two-dimensional S = 1/2 magnetism of $Cu[C_6H_2(COO)_4][C_2H_5NH_3]_2$. *Phys. Rev. B: Condens. Matter Mater. Phys.* **2015**, *91*, 054409.

(16) Woodward, F. M.; Gibson, P. J.; Jameson, G. B.; Landee, C. P.; Turnbull, M. M.; Willett, R. D. Two-Dimensional Heisenberg Antiferromagnets: Syntheses, X-ray Structures, and Magnetic Behavior of $[Cu(pz)_2](ClO_4)_2$, $[Cu(pz)_2](BF_4)_2$, and $[Cu(pz)_2(NO_3)](PF_6)$. *Inorg. Chem.* **2007**, *46*, 4256−4266.

(17) Brown, S.; Cao, J.; Musfeldt, J. L.; Conner, M. M.; McConnell, A. C.; Southerland, H. I.; Manson, J. L.; Schlueter, J. A.; Phillips, M. D.; Turnbull, M. M.; Landee, C. P. Hydrogen Bonding and Multiphonon Structure in Copper Pyrazine Coordination Polymers. *Inorg. Chem.* **2007**, *46*, 8577−8583.

(18) Manson, J. L.; Schlueter, J. A.; Funk, K. A.; Southerland, H. I.; Twamley, B.; Lancaster, T.; Blundell, S. J.; Baker, P. J.; Pratt, F. L.; Singleton, J.; Mcdonald, R. D.; Goddard, P. A.; Sengupta, P.; Batista, C. D.; Ding, L.; Lee, C.; Whangbo, M.-H.; Franke, I.; Cox, S.; Baines, C.; Trial, D. Strong H···F Hydrogen Bonds as Synthons in Polymeric Quantum Magnets: Structural, Magnetic, and Theoretical Characterization of $[Cu(HF_2)(pyrazine)_2]SbF_6$, $[Cu_2F(HF)(HF_2)(pyrazine)_4](SbF_6)_2$, and $[CuAg(H_3F_4)(pyrazine)_5](SbF_6)_2$. *J. Am. Chem. Soc.* **2009**, *131*, 6733−6747.

(19) Manson, J. L.; Schlueter, J. A.; McDonald, R. D.; Singleton, J. Crystal Structure and Antiferromagnetic Ordering of Quasi-2D $[Cu(HF_2)(pyz)_2]TaF_6$ (pyz = pyrazine). *J. Low Temp. Phys.* **2010**, *159*, 15−19.

(20) Macchi, P.; Bürgi, H.-B.; Chimpri, A. S.; Hauser, J.; Gál, Z. Low-energy contamination of Mo microsource X-ray radiation: analysis and solution of the problem. *J. Appl. Crystallogr.* **2011**, *44*, 763−771.

(21) *CrysAlisPro*, Version 171.36.28; Agilent, 2010.

(22) Sheldrick, G. M. A short history of *SHELX*. *Acta Crystallogr., Sect. A: Found. Crystallogr.* **2008**, *64*, 112−122.

(23) Hansen, N. K.; Coppens, P. Testing aspherical atom refinements on small-molecule data sets. *Acta Crystallogr., Sect. A: Cryst. Phys., Diffr., Theor. Gen. Crystallogr.* **1978**, *34*, 909−921.

(24) Volkov, A.; Macchi, P.; Farrugia, L. J.; Gatti, C.; Mallinson, P.; Richter, T.; Koritsanszky, T. *XD2015;* The State University of New York at Buffalo, 2015.

(25) Holladay, A.; Leung, P.; Coppens, P. Generalized relations between *d*-orbital occupancies of transition-metal atoms and electron-density multipole population parameters from X-ray diffraction data. *Acta Crystallogr., Sect. A: Found. Crystallogr.* **1983**, *39*, 377−387.

DOI: 10.1021/acs.inorgchem.7b03150
Inorg. Chem. XXXX, XXX, XXX−XXX

(26) Willmott, P. R.; Meister, D.; Leake, S. J.; Lange, M.; Bergamaschi, A.; Böge, M.; Calvi, M.; Cancellieri, C.; Casati, N.; Cervellino, A.; Chen, Q.; David, C.; Flechsig, U.; Gozzo, F.; Henrich, B.; Jäggi-Spielmann, S.; Jakob, B.; Kalichava, I.; Karvinen, P.; Krempasky, J.; Lüdeke, A.; Lüscher, R.; Maag, S.; Quitmann, C.; Reinle-Schmitt, M. L.; Schmidt, T.; Schmitt, B.; Streun, A.; Vartiainen, I.; Vitins, M.; Wang, X.; Wullschleger, R. The Materials Science beamline upgrade at the Swiss Light Source. *J. Synchrotron Radiat.* **2013**, *20*, 667−682.

(27) Coelho, A. A. *TOPAS Academic,* Version 5; Coelho Software: Brisbane, Australia, 2012.

(28) Fischer, P.; Keller, L.; Schefer, J.; Kohlbrecher, J. The Double axis Multi-Counter (DMC) diffractometer for cold neutrons. *Neutron News* **2000**, *11*, 19−21.

(29) Roisnel, T.; Rodriguez-Carvajal, J. *WinPLOTR,* A Windows Tool for Powder Diffraction Pattern Analysis; Proceedings of the Seventh European Powder Diffraction Conference (EPDIC 7), Scitec, 2000.

(30) Rodriguez-Carvajal, J. Recent advances in magnetic structure determination by neutron powder diffraction. *Phys. B* **1993**, *192*, 55−69.

(31) Dovesi, R.; Saunders, V. R.; Roetti, C.; Orlando, R.; Zicovich-Wilson, C. M.; Pascale, F.; Civalleri, B.; Doll, K.; Harrison, N. M.; Bush, I. J.; D'Arco, P.; Llunell, M.; Causà, M.; Noël, Y. *CRYSTAL14 User's Manual;* University of Torino: Torino, Italy, 2014.

(32) Doll, K.; Harrison, N. M. Chlorine adsorption on the Cu(111) surface. *Chem. Phys. Lett.* **2000**, *317*, 282−289.

(33) Peintinger, M. F.; Oliveira, D. V.; Bredow, T. Consistent Gaussian basis sets of triple-zeta valence with polarization quality for solid-state calculations. *J. Comput. Chem.* **2013**, *34*, 451−459.

(34) Frisch, M. J.; Trucks, G. W.; Schlegel, H. B.; Scuseria, G. E.; Robb, M. A.; Cheeseman, J. R.; Scalmani, G.; Barone, V.; Mennucci, B.; G. A. Petersson, H. N.; Caricato, M.; Li, X.; Hratchian, H. P.; Izmaylov, A. F.; Bloino, J.; Zheng, G.; Sonnenberg, J. L.; Hada, M.; Ehara, M.; Toyota, K.; Fukuda, R.; Hasegawa, J.; Ishida, M.; Nakajima, T.; Honda, Y.; Kitao, O.; Nakai, H.; Vreven; Montgomery, J. A., Jr.; Peralta, J. E.; Ogliaro, F.; Bearpark, M.; Heyd, J. J.; Brothers, E.; Kudin, K. N.; Staroverov, V. N.; Kobayashi, R.; Normand, J.; Raghavachari, K.; Rendell, A.; Burant, J. C.; Iyengar, S. S.; Tomasi, J.; Cossi, M.; Rega, N.; Millam, J. M.; Klene, M.; Knox, J. E.; Cross, J. B.; Bakken, V.; Adamo, C.; Jaramillo, J.; Gomperts, R.; Stratmann, R. E.; Yazyev, O.; Austin, A. J.; Cammi, R.; Pomelli, C.; Ochterski, J. W.; Martin, R. L.; Morokuma, K.; Zakrzewski, V. G.; Voth, G. A.; Salvador, P.; Dannenberg, J. J.; Dapprich, S.; Daniels, A. D.; Farkas, Ö.; Foresman, J. B.; Ortiz, J. V.; Cioslowski, J.; Fox, D. J. *Gaussian 09;* Gaussian, Inc.: Wallingford, CT, 2009.

(35) Cizmar, E.; Zvyagin, S. A.; Beyer, R.; Uhlarz, M.; Ozerov, M.; Skourski, Y.; Manson, J. L.; Schlueter, J. A.; Wosnitza, J. Magnetic properties of the quasi-two-dimensional S = 1/2 Heisenberg antiferromagnet $[Cu(pyz)_2(HF_2)]PF_6$. *Phys. Rev. B: Condens. Matter Mater. Phys.* **2010**, *81*, 064422−064425.

(36) Lancaster, T.; Blundell, S.; Baker, P.; Brooks, M.; Hayes, W.; Pratt, F.; Manson, J.; Conner, M.; Schlueter, J. Muon-Fluorine Entangled States in Molecular Magnets. *Phys. Rev. Lett.* **2007**, *99*, 267601−267604.

(37) Liu, T.; Chen, Y.-H.; Zhang, Y.-J.; Wang, Z.-M.; Gao, S. NaCl-Type Frameworks of $[M(pyrazine)_2NO_2]ClO_4$ (M = Co, Cu), the First Examples Containing $\mu_{1,3}$-Nitrito Bridges Showing Antiferromagnetism. *Inorg. Chem.* **2006**, *45*, 9148−9150.

(38) Manson, J. L.; Conner, M. M.; Schlueter, J. A.; Lancaster, T.; Blundell, S. J.; Brooks, M. L.; Pratt, F. L.; Papageorgiou, T.; Bianchi, A. D.; Wosnitza, J.; Whangbo, M.-H. $[Cu(HF_2)(pyz)_2]BF_4$ (pyz = pyrazine): long-range magnetic ordering in a pseudo-cubic coordination polymer comprised of bridging HF_2^- and pyrazine ligands. *Chem. Commun.* **2006**, *4*, 4894−4896.

(39) Dos Santos, L. H. R.; Lanza, A.; Barton, A. M.; Brambleby, J.; Blackmore, W. J. A.; Goddard, P. A.; Xiao, F.; Williams, R. C.; Lancaster, T.; Pratt, F. L.; Blundell, S. J.; Singleton, J.; Manson, L.; Macchi, P. Experimental and Theoretical Electron Density Analysis of Copper Pyrazine Nitrate Quasi-Low-Dimensional Quantum Magnets. *J. Am. Chem. Soc.* **2016**, *138*, 2280−2291.

(40) Bader, R. W. F. *A Quantum Theory;* Oxford University Press, 1990.

(41) Clarke, S. J.; Harrison, A.; Mason, T. E.; McIntyre, G. J.; Visser, D. Magnetic ordering and fluctuations in the S = 1/2 square Heisenberg antiferromagnet $Cu(DCO_2)_2.4D_2O$. *J. Phys.: Condens. Matter* **1992**, *4*, L71−L76.

(42) Taroni, A.; Bramwell, S. T.; Holdsworth, P. C. W. Universal window for two-dimensional critical exponents. *J. Phys.: Condens. Matter* **2008**, *20*, 275233.

(43) Sengupta, P.; Batista, C. D.; McDonald, R. D.; Cox, S.; Singleton, J.; Huang, L.; Papageorgiou, T. P.; Ignatchik, O.; Herrmannsdörfer, T.; Manson, J. L.; Schlueter, J. A.; Funk, K. A.; Wosnitza, J. Nonmonotonic field dependence of the Néel temperature in the quasi-two-dimensional magnet $[Cu(HF_2)(pyz)_2]BF_4$. *Phys. Rev. B: Condens. Matter Mater. Phys.* **2009**, *79*, 1.

(44) Manson, J. L.; Lapidus, S. H.; Stephens, P. W.; Peterson, P. K.; Carreiro, K. E.; Southerland, H. I.; Lancaster, T.; Blundell, S. J.; Steele, A. J.; Goddard, P. A.; Pratt, F. L.; Singleton, J.; Kohama, Y.; McDonald, R. D.; Del Sesto, R. E.; Smith, N. A.; Bendix, J.; Zvyagin, S. A.; Kang, J.; Lee, C.; Whangbo, M.-H.; Zapf, V. S.; Plonczak, A. Structural, Electronic, and Magnetic Properties of Quasi-1D Quantum Magnets $[Ni(HF_2)(pyz)_2]X$ (pyz = pyrazine; X = PF_6^-, SbF_6^-) Exhibiting Ni-FHF-Ni and Ni-pyz-Ni Spin Interactions. *Inorg. Chem.* **2011**, *50*, 5990−6009.

(45) Landee, C. P.; Turnbull, M. M. A gentle introduction to magnetism: units, fields, theory, and experiment. *J. Coord. Chem.* **2014**, *67*, 375−439.

(46) Yasuda, C.; Todo, S.; Hukushima, K.; Alet, F.; Keller, M.; Troyer, M.; Takayama, H. Néel Temperature of Quasi-Low-Dimensional Heisenberg Antiferromagnets. *Phys. Rev. Lett.* **2005**, *94*, 217201.

(47) Woodward, F. M.; Albrecht, A. S.; Wynn, C. M.; Landee, C. P.; Turnbull, M. M. Two-dimensional S = 1/2 Heisenberg antiferromagnets: Synthesis, structure, and magnetic properties. *Phys. Rev. B: Condens. Matter Mater. Phys.* **2002**, *65*, 144412.

(48) Matsumoto, T.; Miyazaki, Y.; Albrecht, A. S.; Landee, C. P.; Turnbull, M. M.; Sorai, M. Heat Capacities of the *S* = 1/2 Two-Dimensional Heisenberg Antiferromagnet Bis(2-amino-5-chloropyridinium) Tetrabromocuprate(II) $[(5CAP)_2CuBr_4]$ and Its Diamagnetic Analogue $[(5CAP)_2ZnBr_4]$. *J. Phys. Chem. B* **2000**, *104*, 9993−10000.

(49) Day, P. *Electronic Structure and Magnetism of Inorganic Compounds;* The Chemical Society: Great Britain, 1977; Vol. 5.